Journal of Sound and Vibration (2000) **232**(2), 449–471
doi:10.1006/jsvi.1999.2748, available online at http://www.idealibrary.com on IDEAL®

VIBRATION ANALYSIS OF A THIN-PLATE BOX USING A FINITE ELEMENT MODEL WHICH ACCOMMODATES ONLY IN-PLANE MOTION

R. M. Grice and R. J. Pinnington

Institute of Sound and Vibration Research, University of Southampton, Southampton, SO17 1BJ, England

(*Received* 12 *May* 1999, *and in final form* 12 *October* 1999)

Many practical built-up structures, e.g., the modern car body, are essentially assemblies of numerous thin plates joined at many edges. The plates are often so thin that they cannot support appreciable loads out of plane. In the case of a car, the body can only support the static loads of either the vehicle or the engine using the substantial in-plane stiffness of the plates. During operation of the vehicle, the dynamic loads applied to the body by the engine and suspension also act in-plane so that the vibrational power injected into the body is controlled by the in-plane properties. The paper argues that under such conditions, the vibrational response of the structure must be dominated by the mobility of long wavelength in-plane waves. To investigate this hypothesis, a six-sided thin-plate box excited by a force at a stiff point where two sides meet is chosen as the test structure. A finite element model of the box is constructed from membrane elements which accommodate only in-plane response. Predictions of the input and transfer frequency response of the box are compared with laboratory measurements with favourable agreement. The finite element model is advantageous because it has relatively few degrees of freedom making it computationally attractive, yet remains valid over very broad frequency ranges. It could therefore be used during the preliminary stages of the design of a practical thin-plate built-up structure.

1. INTRODUCTION

This paper presents a finite element model which predicts the frequency response of a six-sided thin-plate box using only its in-plane motion. The model is targeted at engineering applications which require the vibration analysis of built-up thin-plate structures such as a car body.

The modern car body is essentially an assembly of thin plates joined at many edges. The plates are so thin, typically less than 1·5 mm [1], that they cannot support appreciable loads out of plane. In particular, they can only support the static loads of either the vehicle or the engine using their substantial in-plane stiffness. During operation of the vehicle, the dynamic loads applied to the body by the engine and suspension also act in-plane so that the vibrational power injected into the body must be controlled by the in-plane properties [2]. Specifically, the injected power is carried from the engine and suspension attachment points by long-wavelength in-plane quasi-longitudinal and in-plane shear waves [3]. The high in-plane stiffness of the plates means that these waves propagate with high-phase speeds throughout the structure and in doing so impinge on the numerous joints between plates. At these joints the in-plane waves generate other in-plane waves as well as flexural waves in adjoining plates. The flexural waves have much shorter wavelengths than the in-plane

0022-460X/00/170449 + 23 $35.00/0

waves on account of the small flexural stiffness of the plates. Some of the energy of the long-wavelength in-plane waves is used to generate the short-wavelength flexural waves which therefore damp the long-wavelength response. In this manner, the vibrational field in the car body develops into a complicated mixture of long- and short-wavelength waves [4]. Henceforth for brevity, the terms *long wave* and *short wave* will be used instead of *long-wavelength wave* and *short-wavelength wave* respectively.

The relative proportions of the total power carried by the two waves depend on the inherent damping of the long waves (e.g., the material loss factor) and the amount of coupling between the two waves at the structural joints. This means that the damping of the long waves can be increased if more energy can be transmitted to the short waves. This is particularly significant in the car body where the inherent damping of the long in-plane waves is usually quite low because the structure is damped using loosely fitting treatments such as rubber foam and carpet. These have little impact on the in-plane waves since both the interfacial pressure and the coefficient of friction between the treatments and the structure are small [5].

Of course, the engine and suspension are not the only sources of vibration in a modern car. In general, noise and vibration originates from the power train, road surface excitation of the tyres and suspension, and aerodynamic excitation of the body [6]. These sources include both a random contribution from road and aerodynamic excitation together with a tonal contribution from the power train. Below 500 Hz the structural vibration of the body and the sound pressure level inside the passenger compartment are dominated by transmission of the second order harmonic of the engine speed through the engine isolators and from transmission of road vibration through the suspension mounting points [7]. At present, car manufacturers use finite element models of a car body with upwards of 250 000 degrees of freedom to predict the structural vibration [8]. These models, which include both in-plane and flexural motion, predict the lowest modes of the car body up to about 100 Hz and typically require overnight run times even on the fastest super-computers presently available. Consequently, the analysis times and costs involved in refining the body design to meet desired interior and exterior noise targets are gargantuan. However, the previous description of the dynamics of the long and short waves in a built-up structure suggests that in the region below 500 Hz where the structural excitation is dominated by transmission from the engine and suspension, the structural response can be estimated using only the dominant in-plane motion. Moreover, because the in-plane wavelengths are so much greater than the flexural wavelengths, a finite element model which accommodates only in-plane motion will require far fewer elements (and thus degrees of freedom) than the model which accommodates both in-plane and flexural motion. Of course, such an in-plane model is unlikely to be as accurate as a model which includes both in-plane and flexural motions. Nevertheless, it should prove cost-effectiveness during preliminary design stages.

To investigate the hypothesis that a finite element model which accommodates only in-plane motion can estimate the response of a built-up structure, a six-sided thin-plate perspex box shown in Figure 1 is chosen as the test structure. The box is driven at the mid-point of one joint by a point force as shown. This force acts in the plane of one of the plates and normal to the plane of the other plate, thereby replicating the direct excitation of a car body by the engine and suspension. The geometry of the box in Figure 1 was determined from two considerations. First, the plates were kept flat so that in-plane and flexural waves travelling in their interior are uncoupled [3]. Second, the overall dimensions of the box were determined from the current limit in the vibration analysis of internal combustion engines which is currently around 3 kHz [9]. It would be useful if the in-plane model could be analyzed as far as this frequency in order to provide greater scope for future applications. Because of the differences in the phase speeds of waves in perspex and steel

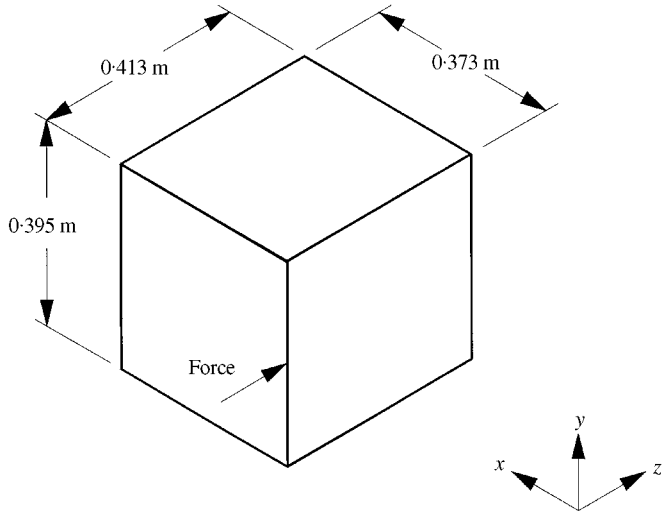

Figure 1. Sketch of the thin-plate perspex box driven by a point harmonic force at the middle of one edge where two sides meet. All sides are 5 mm thick. The material properties are given in Table 1.

plates, analysis at 3 kHz of a 1 mm thick steel plate box with sides of length 2 m (dimensions which are characteristic of a car body [1]) is equivalent to the analysis of a perspex box with sides of length 0·35 m at 6 kHz. Thus, the in-plane finite element model of the perspex box will be analyzed up to 6 kHz.

The objective of the paper is to present a finite element model of the box which accommodates only in-plane motion and compare its predictions of input and transfer frequency response with laboratory measurements. The layout of the paper is as follows. Section 2 examines the characteristic mobilities of the different waves which may propagate in the box and shows that the long in-plane waves control both the power injected into it and the power transmitted around it. Section 3 quantifies the dissipation of energy in the structure by examining a balance between the inherent damping of the in-plane waves and the power transmitted to the short flexural waves at the structural joints. Section 4 details the construction of a finite element mesh which accommodates only the in-plane motion of the box. Section 5 describes the laboratory measurements and section 6 compares these measurements with the input and transfer frequency response functions predicted by the finite element mesh.

2. THE CHARACTERISTIC MOBILITIES OF A THIN-PLATE BOX

This section begins by describing the waves which can propagate in a thin uniform plate. These waves are then used to characterize the mobilities of the perspex box.

2.1. WAVENUMBERS FOR WAVES IN A THIN PLATE

For harmonic excitation with time dependence $e^{j\omega t}$ where ω is the radian frequency, the wavenumber k_{LI} for quasi-longitudinal waves [3] in a thin plate of thickness t is

$$k_{LI} = \omega \sqrt{\frac{m_p''}{D_{LI}}}, \quad m_p'' = \rho t, \quad D_{LI} = \frac{Et}{(1 - \nu^2)}, \tag{1}$$

TABLE 1

Typical material properties of steel and perspex

Material	Steel	Perspex
Young's modulus (GN/m^2)	210	4·7
Density (kg/m^3)	7850	1192
Poisson's ratio	0·3	0·3
Loss factor	0·001	0·05

where E, ρ, v are the Young's modulus, density and Poisson's ratio respectively and m_p'' is the plate mass per unit area (see Appendix A for list of symbols). The in-plane stiffness D_{LI} is very high and so quasi-longitudinal waves have high phase speeds. A thin uniform plate can also carry in-plane shear waves having a wavenumber k_s and stiffness D_s,

$$k_s = \omega\sqrt{\frac{m_p''}{D_S}}, \quad D_S = \frac{Et}{2(1+v)}. \tag{2}$$

Both waves are non-dispersive and are sometimes called *high impedance* waves.

The wavenumber k_{FI} for Euler–Bernoulli flexural waves in the plate is

$$k_{FI} = \sqrt{\omega}\left(\frac{m_p''}{D_{FI}}\right)^{1/4}, \quad D_{FI} = \frac{Et^3}{12(1-v^2)}, \tag{3}$$

where D_{FI} is the stiffness per unit width. The phase speed of Euler–Bernoulli waves is generally much less than either of the in-plane waves but rises with $\sqrt{\omega}$ because flexural waves are dispersive. They are sometimes called *low impedance* waves.

Figure 2 shows dispersion curves for all three wave types in 1 mm steel and 5 mm perspex plates having the material properties of Table 1. Figure 2 shows that at any frequency, the quasi-longitudinal wave has the lowest wavenumber. The in-plane shear wavenumber is approximately 1·6 times the quasi-longitudinal wavenumber. The flexural wavenumber is much higher across the bandwidth shown.

For the thin plates being considered here, the ratio of the flexural wavenumber to the quasi-longitudinal wavenumber is

$$\frac{k_{FI}}{k_{LI}} = \frac{1}{\sqrt{\omega t}}\left[\frac{12E}{\rho(1-v^2)}\right]^{1/4}. \tag{4}$$

This ratio is a function of thickness and decreases with frequency. Applying this relation to the previously considered steel and perspex plates, for the steel plate at say 1 kHz, the flexural wavenumber is more than 50 times the quasi-longitudinal wavenumber while for the perspex plate at the same frequency, the flexural wavenumber is about 15 times the quasi-longitudinal wavenumber.

2.2. THE CHARACTERISTIC INPUT MOBILITIES OF THE BOX

The thin-plate box of Figure 1 can be viewed as a set of flat plates which meet at right angles. Along the edges two plates meet and at the corners three plates meet. However, one can consider the corner to consist of one plate bent into an L-shape and wrapped around

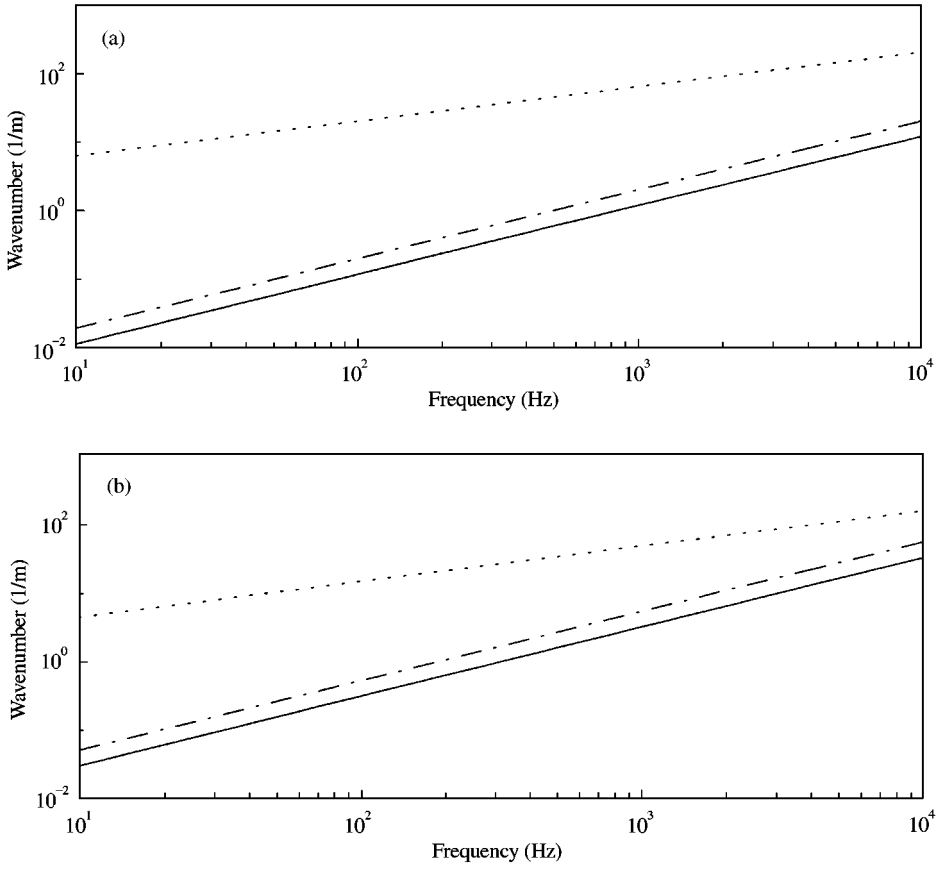

Figure 2. Dispersion curves for the waves in thin uniform infinite steel and perspex plates having material properties of Table 1: —— in-plane quasi-longitudinal; - ·- · - · in-plane shear; ....., flexural. (a) 1 mm mild steel plate; (b) 5 mm perspex plate.

another plate. In this way, the corners and edges can be idealized as an assembly of just two components. Thus, a force applied at any joint as in Figure 1 drives at least one plate in plane and one plate in flexure. Let the component being driven in plane be called the *in-plane component* and the component driven in flexure be called the *out-of-plane component*. Both components have width b normal to the joint and thickness t. The following subsections describe the characteristic mobilities of the in-plane and out-of-plane components initially when uncoupled, and subsequently when coupled together.

2.2.1. *Characteristic mobility of the in-plane component by itself*

The in-plane component behaves dynamically like a rod provided that all plane sections which are normal to its axis remain plane or nearly plane. This occurs when the phase change across the width of the rod satisfies $k_L b \ll 1$ where k_L is the wavenumber for longitudinal waves. Its characteristic input mobility $\tilde{Y}_L^{1/2\infty}$ is then [3]

$$Y_L^{1/2\infty} = \frac{1}{m_b' c_L}, \quad c_L = \sqrt{E/\rho}, \tag{5}$$

where c_L is the non-dispersive phase speed for longitudinal waves in a rod.

At higher frequencies the phase change across the width increases and the in-plane component behaves increasingly like a plate. The precise input mobility will depend upon the mode shape across the width but its characteristic mobility tends to that of a semi-infinite plate [10]

$$Y_{LI}^{1/2\infty} = \frac{\omega}{4D_{LI}} + \frac{\omega}{4D_S}. \tag{6}$$

The first term in this equation is the mobility of a semi-infinite plate-driven in-plane carrying quasi-longitudinal waves. The second term accounts for the mobility due to shear waves. This result has been verified experimentally in reference [2] and will henceforth be referred to as *membrane mobility* of the in-plane component.

At higher frequencies still, when the phase change across the thickness of the plate is significant the plate behaves like a semi-infinite half-space. For the perspex and steel plates whose dispersion curves are shown in Figure 2, the transition to half-space behaviour occurs at 66 kHz (perspex) and 1 MHz (steel) which are far too high to be of interest at present.

2.2.2. *Characteristic mobility of the out-of-plane component by itself*

At low frequencies when the phase change across the width of the out-of-plane component is small, i.e., $k_F b \ll 1$ where k_F is the wavenumber for flexural waves in an Euler–Bernoulli beam, its characteristic mobility is that of a semi-infinite beam $\tilde{Y}_F^{1/2\infty}$ [3]:

$$\tilde{Y}_F^{1/2\infty} = \frac{1}{m_b' c_F}(1-j), \quad c_F = \sqrt{\omega}\left(\frac{D_F}{m_b'}\right)^{1/4}, \quad D_F = \frac{Ebt^3}{12}. \tag{7}$$

Here, m_b' is the mass per unit length of the beam and c_F is the dispersive phase speed. This mobility falls with $\sqrt{\omega}$. At higher frequencies when the width-ways phase change is significant, the characteristic mobility changes to that of a semi-infinite plate driven by a force on its free edge [3]:

$$Y_{FI}^{1/2\infty} = \frac{1}{3{\cdot}5\sqrt{m_p'' D_{FI}}}. \tag{8}$$

The mobility of equation (8) is a constant and will be referred to as the *plate mobility*. At very high frequencies when the through-thickness phase change becomes significant the beam will deform in transverse shear. The mobility of transverse shear waves is higher than that of flexural waves [3]. The frequency at which this change in behaviour occurs in the structures considered here is also very high. For the perspex and steel plates these frequencies are 20 kHz (perspex) and 200 kHz (steel).

Figure 3(a) compares the characteristic mobilities of the rod, membrane, beam and plate [equations (5)–(8)] based on the dimensions of the perspex box, and Figure 3(b) shows these four mobilities for a 1 mm steel box with a side length of 2 m. It can be seen that in general the beam and plate mobilities exceed those of the rod and membrane.

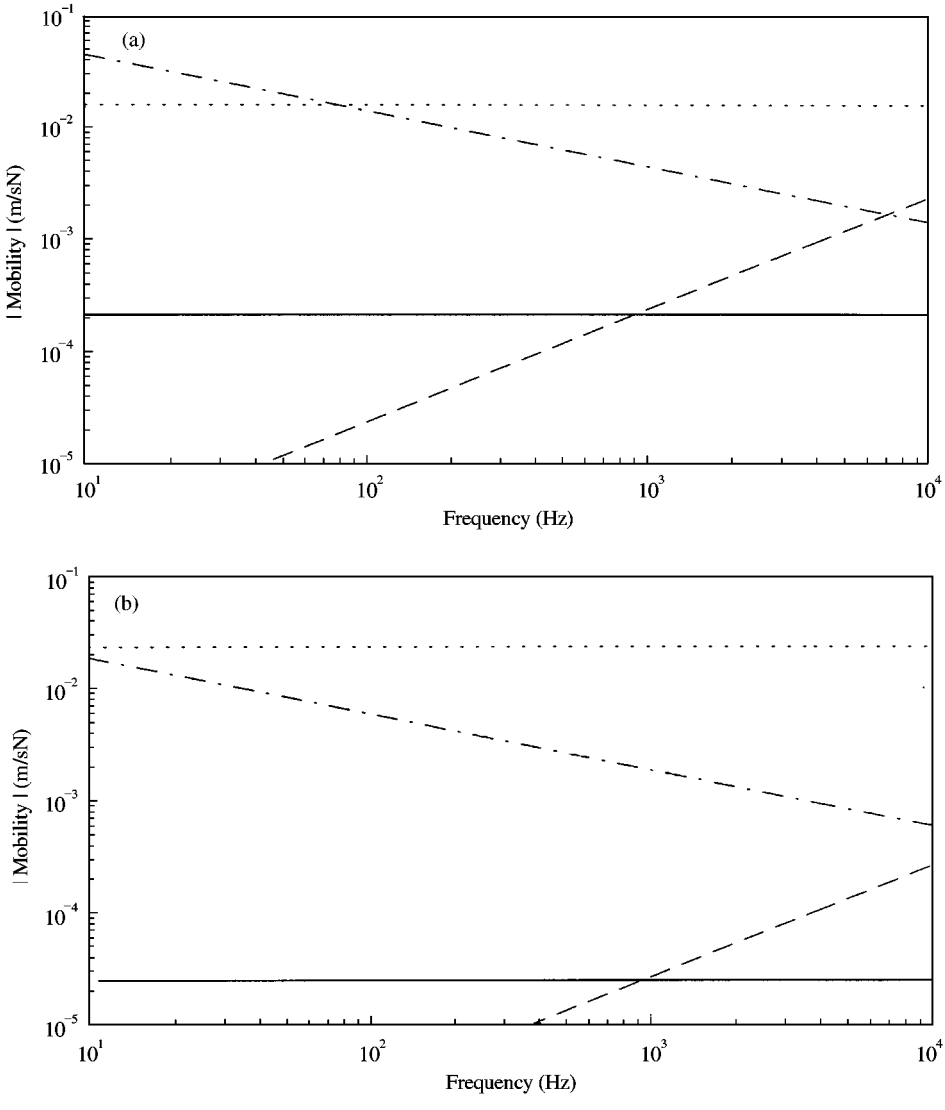

Figure 3. The approximate characteristic input mobilities of the two plates meeting at the drive point in Figure 1 for perspex and steel materials: —— rod; - - -, membrane; - ·- · - ·. beam; ....., plate. (a) Perspex, thickness 5 mm, width 0·395 m; (b) steel, thickness 1 mm, width 2 m.

2.2.3. *Characteristic mobility of the coupled in-plane and out-of-plane components*

When the two components are coupled as in Figure 1 along the joint on which the force acts, their individual impedances add and so the input mobility becomes

$$\tilde{Y}_C = \frac{\tilde{Y}_1 \tilde{Y}_2}{(\tilde{Y}_1 + \tilde{Y}_2)}. \tag{9}$$

This relationship shows that if either of the component mobilities $\tilde{Y}_1$, $\tilde{Y}_2$ is much larger than the other, the coupled input mobility will tend strongly toward the *lower* component

mobility which constrains the coupled response to its own level. Thus, from Figure 3, it can be seen that at low frequencies when the component mobilities are those of the rod and beam, the coupled mobility is

$$\tilde{Y}_C = \frac{Y_L^{1/2\infty}\, Y_F^{1/2\infty}}{(Y_L^{1/2\infty} + Y_F^{1/2\infty})} \approx Y_L^{1/2\infty}, \tag{10}$$

i.e., it is dominated by the in-plane mobility. At higher frequencies when the component mobilities are those of the membrane and plate, the coupled mobility is

$$\tilde{Y}_C = \frac{Y_{LI}^{1/2\infty}\, Y_{FI}^{1/2\infty}}{(Y_{LI}^{1/2\infty} + Y_{FI}^{1/2\infty})} \approx Y_{LI}^{1/2\infty}, \tag{11}$$

i.e., the in-plane mobility still dominates over the frequency range shown. Moreover, Figure 3 shows that there is in general a large mobility mismatch between the in-plane and flexural waves. This implies that the amount of energy transferred from one wave type to the other at joints will be small [11], thereby retaining much of the vibrational energy within the in-plane waves. Hence, the transmission of vibrational energy around the edge-excited box (and therefore its transfer mobility to other edges) will also be controlled by the mobility of the in-plane motion.

The characteristic input mobility of the edge-excited box will be similar to the input mobility of the two plates meeting at the drive point except that at low frequencies the mobility will be that of a rigid mass. In the region above the rigid-body response the characteristic mobility will revert to the membrane mobility of equation (6).

In summary, it can be seen that because the in-plane waves are so much longer than the flexural waves, the response of the edge-excited box is characterized by its membrane mobility (or impedance) over a broad frequency range. This is true for both the perspex box and a practical car body manufactured from 1 mm steel plates.

3. THE DISTRIBUTION OF ENERGY BETWEEN IN-PLANE AND FLEXURAL WAVES IN THE THIN PLATE BOX

As mentioned in section 1, the energy level of the in-plane waves in a built-up structure is influenced by the inherent material loss factor and the amount of energy which is transmitted to flexural waves at the joints. An estimate of the relative importance of these two dissipation processes can be obtained by considering a power balance between the power input to the box and the power dissipated. Figure 4 shows a two sub-system model of the box. Sub-system I represents the in-plane waves. Time-averaged power $\bar{P}_{IN}$ is injected directly into the in-plane waves from the external excitation. Sub-system F represents the flexural waves. Assuming that the joints are non-dissipative, power balance requires that

$$\bar{P}_{IN} = \eta_I \omega \bar{E}_I + \eta_F \omega \bar{E}_F. \tag{12}$$

If the box has roughly equal side lengths L in all three axes, the total energy of the in-plane motion can be approximated by

$$\bar{E}_I \approx \|\tilde{v}_I^2\| (6 m_p'' L^2), \tag{13}$$

where $\|v_I^2\|$ is the spatially averaged mean-square velocity of the in-plane waves.

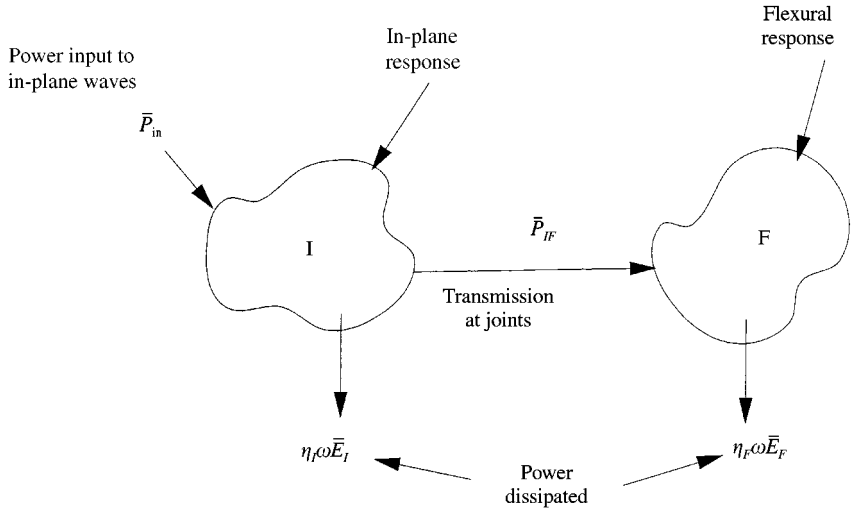

Figure 4. Model of the energy dissipation mechanisms in a built-up thin-plate structure.

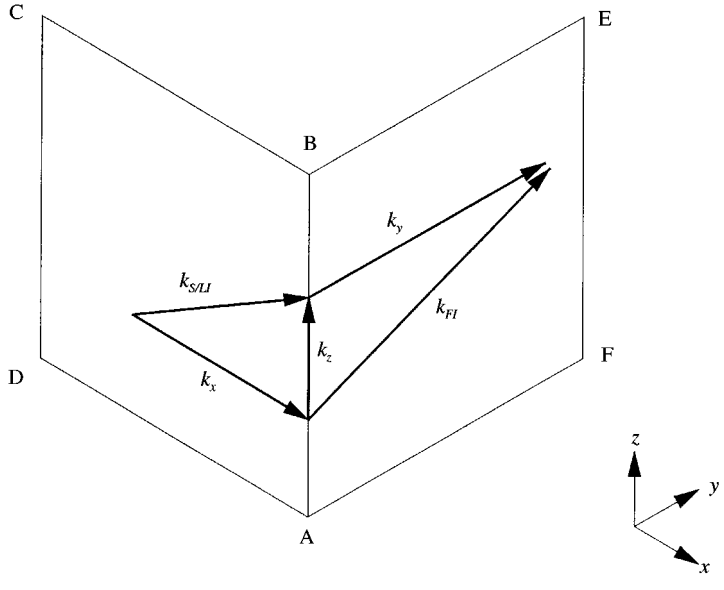

Figure 5. Wavenumber vector triangles for the transmission of in-plane and flexural waves across a joint between two plates.

To determine the power transmitted to the plates in flexure $\bar{P}_{IF}$ consider Figure 5. This shows one side of the box *ABCD* carrying an in-plane wave with wavenumber $k_{S/LI}$ (where the subscript implies any in-plane wave type) and one other side *ABEF* which is shown carrying a flexural wave k_{FI}. At the joint *AB* these two waves trace match. In general, the in-plane waves transmit power to the flexural waves which radiate into the four plates attached at right angles to the plate *ABCD*. Because the in-plane waves dominate the mobility at the joints, they act like velocity sources when driving the attached plates in

flexure. Hence, the total power $\bar{P}_{IF}$ injected by the in-plane waves into all the flexural waves across all four edges of each of the six sides of the box can be estimated as

$$\bar{P}_{IF} = \|\tilde{v}_I^2\| \operatorname{Re}\{24L\tilde{Z}_F'\}, \tag{14}$$

where $\tilde{Z}_F'$ is the impedance per unit length of the plate driven in flexure at the edge AB.

To determine the form of the impedance in equation (14) consider the wavenumbers at the joint AB. The flexural wavenumber k_{FI} trace-matches with k_z, i.e.,

$$k_{FI} = \sqrt{k_z^2 + k_y^2}, \tag{15}$$

where k_y is the component of the flexural wavenumber normal to the joint. Figure 2 shows that over the frequency range considered $k_{S/LI} \ll k_{FI}$ so that $k_z \ll k_y$ in equation (15). Thus, the flexural waves radiate into plate $ABEF$ almost normal to the joint AB. This means that the flexural waves present a locally-reacting impedance to the in-plane waves at the joints [12]. Now, in the frequency average, all the power transmitted to the flexural waves is dissipated within the plates. This will be especially valid if the flexural wave loss factor is high due to attached damping treatments such as those applied to the plates of a practical car body in an effort to increase its damping. The impedance per unit width of the plate into which the flexural waves radiate can therefore be approximated by the locally-reacting impedance of a semi-infinite beam [3] involving wavenumber k_{FI},

$$\tilde{Z}_F' = \frac{m_p''\omega}{2k_{FI}}(1 + j). \tag{16}$$

Thus, the power input to the box at the drive point can be approximated by

$$\bar{P}_{IN} = 6\eta_I \omega m_p'' L^2 \|\tilde{v}_I\|^2 + \frac{12\|\tilde{v}_I\|^2 m_p'' \omega L}{k_{FI}}. \tag{17}$$

Equation (17) illustrates the balance between the total power injected into the structure, the power dissipated by the inherent in-plane damping, and the power transmitted to the flexural waves at the joints. By equating the two terms on the right-hand side of equation (17), an estimate can be made of the frequency at which the energy dissipated by the inherent in-plane damping equals that transmitted to the flexural waves at the joints, i.e., the frequency at which $\eta_I \omega \bar{E}_I = \eta_F \omega \bar{E}_F$ in equation (12). Hence, from equation (17) and substituting for the flexural wavenumber from equation (3), this frequency $f_{I=F}$ is

$$f_{I=F} = \frac{2}{\pi \eta_I^2 L^2} \sqrt{\frac{D_{FI}}{m_p''}}. \tag{18}$$

Two observations can be made: (i) if the inherent in-plane loss factor is low, the energy lost to flexural waves is important in damping the in-plane waves *below* the frequency $f_{I=F}$; and (ii) if the inherent in-plane damping is low, the dissipation of energy in the structure could in practice be increased at frequencies below the frequency $f_{I=F}$ by increasing the total joint length.

The frequency $f_{I=F}$ is therefore a parameter which can be used to decide on appropriate vibration control methods. Applying equation (18) to the perspex box with the material properties of Table 1 and an average joint length of 0·394 m, the frequency below which the damping produced by transmission to flexural waves is greater than the inherent in-plane damping is estimated as 4·9 kHz. For a 1 mm steel box with an average joint length of 2 m, the frequency is over 240 kHz. Of course, a practical car body has a much greater total joint

length than a six-sided box, so the frequency below which the damping in the structure is dominated by the power transmitted to flexural waves will be much less than 240 kHz. Nevertheless, this argument indicates that the damping produced by the transmission of in-plane energy to flexural waves at joints is important in dissipating the energy of the in-plane waves in practical structures in the frequency ranges of interest.

4. FINITE ELEMENT ANALYSIS OF THE IN-PLANE MOTION OF THE PERSPEX BOX

The previous sections established the dominance of the in-plane waves on the response of edge-excited thin-plate structures. This section describes the construction of a finite element model which accommodates only the dominant in-plane vibration.

4.1. WAVE PROPAGATION IN A MEMBRANE

Wave motion in a structure relies on the propagation of energy which is stored in its material as kinetic and potential energies. The kinetic energy depends on the mass and velocity. The potential energy depends on the stiffness and strain. A *membrane* is a structure which generally supports only in-plane motion, although it can support out-of-plane motion if in-plane tension exists [13]. A *tensionless* membrane cannot support out-of-plane wave motion because there is no mechanism for storing the appropriate strain energy. This suggests that if a finite element model of the perspex box were constructed using membrane elements which lack flexural stiffness, flexural wave motion would be eliminated in the interior of its plates. Of course, at the edges of the box the in-plane motion in one plate will create out-of-plane motion in any adjoining non-co-planar plate, but this will be unable to create a propagating wave. The following sections detail the construction of such a finite element model.

4.2. MEMBRANE ELEMENT

Finite element analysis programs (see e.g., reference [14]) typically provide a quadrilateral membrane element with four corner nodes. Each node has three degrees of freedom, two in-plane and one out-of-plane but there is no stiffness associated with the out-of-plane degree of freedom [14]. The shape functions for the in-plane degrees of freedom are [14]

$$u = \sum_{i=1}^{4} N_i u_i + \varepsilon_1(1 - p^2) + \varepsilon_2(1 - q^2),$$

$$w = \sum_{i=1}^{4} N_i w_i + \varepsilon_3(1 - p^2) + \varepsilon_4(1 - q^2), \tag{19}$$

where the functions N_i take the general form

$$N_1 = \tfrac{1}{4}(1 - p)(1 - q), \quad N_2 = \tfrac{1}{4}(1 + p)(1 - q),$$

$$N_3 = \tfrac{1}{4}(1 + p)(1 + q), \quad N_4 = \tfrac{1}{4}(1 - p)(1 + q), \tag{20}$$

and u, w are the displacements in the elemental p and q directions respectively. The last two terms in equation (19) improve the ability of the element to mimic in-plane bending with ε_1–ε_4 being generalized co-ordinates associated with the displacement in the interior of the element [15]. These terms increase the elemental accuracy without increasing the number of nodal degrees of freedom but render it non-conforming. The shape function for the out-of-plane degree of freedom is analagous to those shown in equation (19) but without the extra terms.

The finite element program requires values for Young's modulus, density and Poisson's ratio. The material hysteretic loss factor is specified in terms of the equivalent viscous loss factor according to the relationship

$$\eta = 2\zeta. \tag{21}$$

4.3. MAXIMUM FREQUENCY OF INTEREST AND ELEMENTAL DIMENSIONS

In section 2, Figure 3 demonstrated that the characteristic mobility of the perspex box was dominated by the in-plane waves up to at least 10 kHz. For the reasons given in section 1, the maximum frequency which was chosen for the finite element analysis was selected as 6 kHz. This means that both the in-plane quasi-longitudinal and shear waves must be accurately described at this frequency.

Petyt [15] suggests that in modal analysis a minimum of six linear elements per wavelength are required to achieve accuracy better than 1% when predicting natural frequencies. However, it is arguable that this level of accuracy is not required at high frequencies because the natural frequencies of any practical structure will be sensitive to geometric and material tolerance [16]. Petyt's results show that an accuracy in natural frequency prediction of roughly 6% is achievable using four elements per wavelength, although no comment is made concerning possible enhancement using the extra shape functions in equation (19). It was therefore decided to use four elements per wavelength for the mesh of the box.

Since in-plane shear waves have slightly shorter wavelengths than in-plane quasi-longitudinal waves, the element size must be determined from the shear wavelength at 6 kHz. Using the dispersion curve of Figure 2(b) and the dimensions of the box from Figure 1, the longest element side wave calculated to be 0.0516 m which represents a frequency limit of 5961 Hz. However, the quasi-longitudinal waves can actually be modelled to a higher frequency than the shear waves using this element size. The elemental edge length means that quasi-longitudinal waves can be modelled up to 10 082 Hz. It was therefore decided to analyze the model up to 10 kHz. This would provide an interesting opportunity to observe any change in the performance of the mesh above 6 kHz where the shear motion was not well described.

4.4. THE FINITE ELEMENT MESH

The finite element mesh of the box is shown in Figure 6. The numbered arrows indicate nodes which will be referred to subsequently. The thin lines in the interior of the plates indicate the element edges. The mesh contained 386 nodes with 1158 degrees of freedom which is very modest number of degrees of freedom considering the very high bandwidth over which the predictions are to be calculated. An harmonic force of unit magnitude was

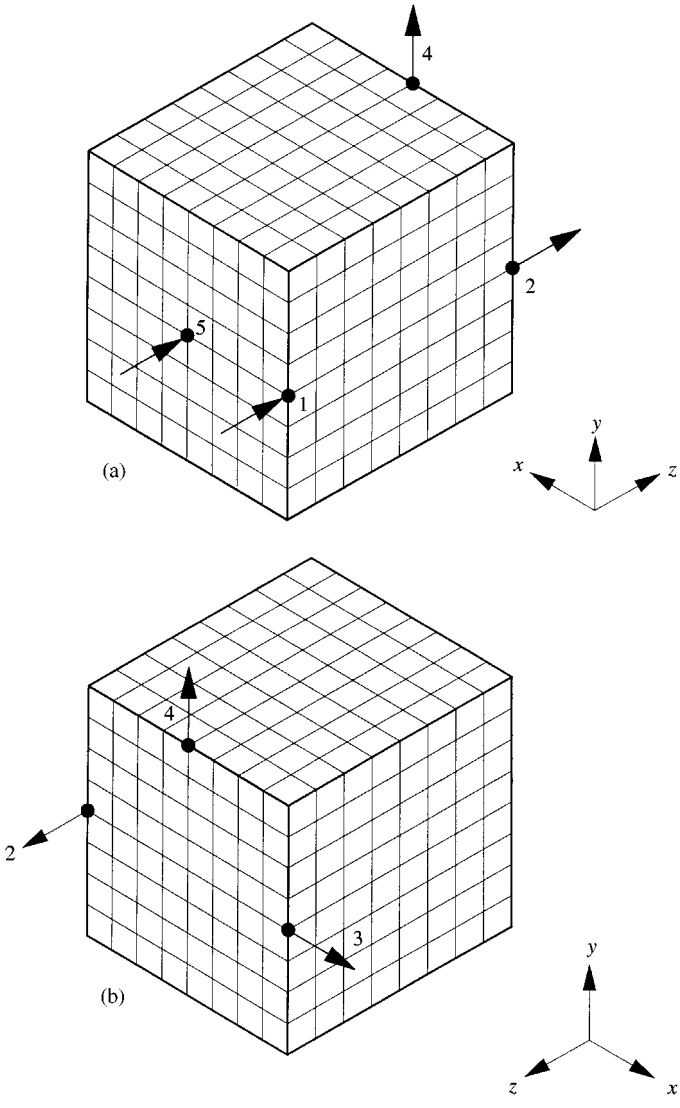

Figure 6. The membrane model of the perspex box. The box is driven by a force at node 1 in the z direction. Nodes 2–5 are referenced in the text. (a) Front view; (b) rear view.

applied at node 1 in the z direction. Henceforth, this mesh will be referred to as the *membrane mesh.*

The frequency response functions of the box were calculated using forced response directly because of the small number of degrees of freedom in the mesh. A frequency range of 100 Hz–10 kHz was used with an increment of 10 Hz. The forced response took just 30 min using a 300 MHz personal computer.

5. LABORATORY MEASUREMENTS ON A PERSPEX BOX

This section describes the procedure used to make laboratory measurements of the input and transfer accelerance (i.e., the ratio of acceleration to force) of the perspex box.

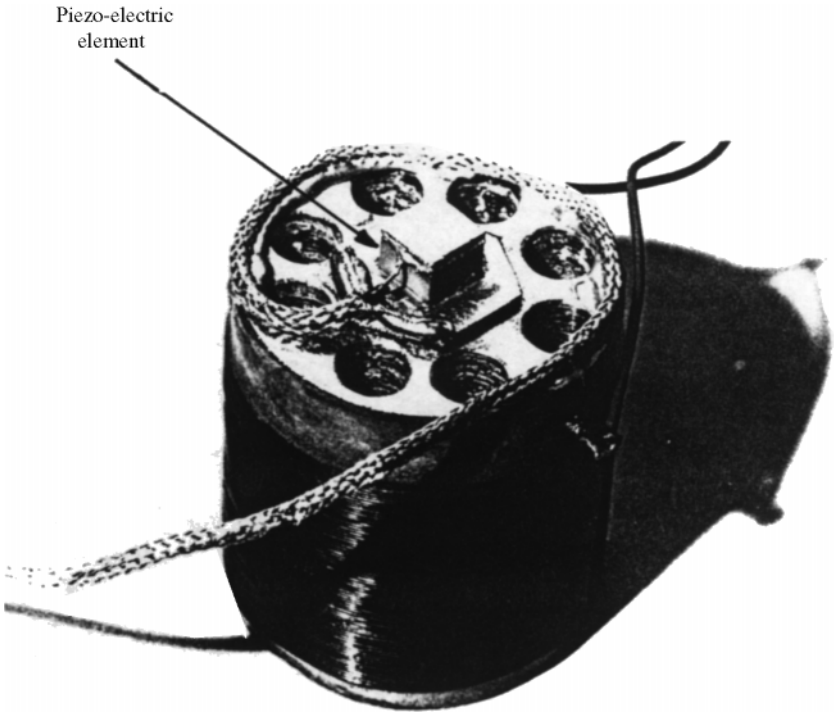

Figure 7. Photograph of the electrodynamic exciter using a tiny piezo-electric element for the force gauge.

The perspex box in Figure 1 had been constructed some five years before the present measurements were made. The box had nominal dimensions to the mid-plane of its sides of $413\,\text{mm} \times 395\,\text{mm} \times 373\,\text{mm}$ with a tolerance of $\pm 2\,\text{mm}$. The plate was nominally 5 mm thick. The sides of the box had been glued together using a proprietary perspex adhesive called TENSOL [17]. The box was placed on a sheet of rubber foam on the supporting bench, thereby isolating it from the bench above the natural frequency created by the mass of the box and the stiffness of the foam. The force was applied at the joint between two sides as in Figure 1 to mimic the loading of the membrane mesh.

The excitation force was applied using two methods. The first method used a conventional impact hammer but the usable frequency range was less than 4 kHz which was insufficient to verify the full range of the predictions. The second method used a lightweight electromagnetic exciter shown in Figure 7. In order to minimize the effects of added mass at the drive-point, this device used a tiny $5\,\text{mm} \times 5\,\text{mm} \times 3\,\text{mm}$ piezo-electric element as the force gauge. A lightweight Brüel & Kjær type 4374 accelerometer with a mass of about 1 g (including the mass of a small length of cable) was attached on the joint close to the drive point using beeswax. It was not possible to mount the accelerometer exactly at the drive point because of the presence of the exciter coil and so the accelerometer was located 19 mm along the joint from the centre of the force gauge.

The exciter was driven using a random signal generated by a digital spectrum analyser which was also used to acquire the measurement data. In all cases, the ordinary coherence function was checked to ensure the data were of acceptable quality.

6. PRESENTATION AND DISCUSSION OF RESULTS

This section compares the measurements on the perspex box with the membrane mesh predictions.

6.1. INPUT ACCELERANCE

Figure 8 compares the predicted input accelerance at node 1 in the z direction with the measurement made using the exciter. The following observations are made.

(i) The two curves are in good agreement in the region of rigid-body response below 320 Hz.

(ii) Above the anti-resonance at 320 Hz the two curves show a similar stiffness-like trend and rise at the same rate. The frequency average value of the measurement is consistently about 3 dB lower than predicted. There are three prominent resonances between 800 Hz and 2 kHz which differ between measurement and prediction by approximately 5%.

(iii) The measurement shows additional poorly defined resonances below 3 kHz which are not predicted. These resonances can be attributed to flexural waves which of course the membrane mesh excludes.

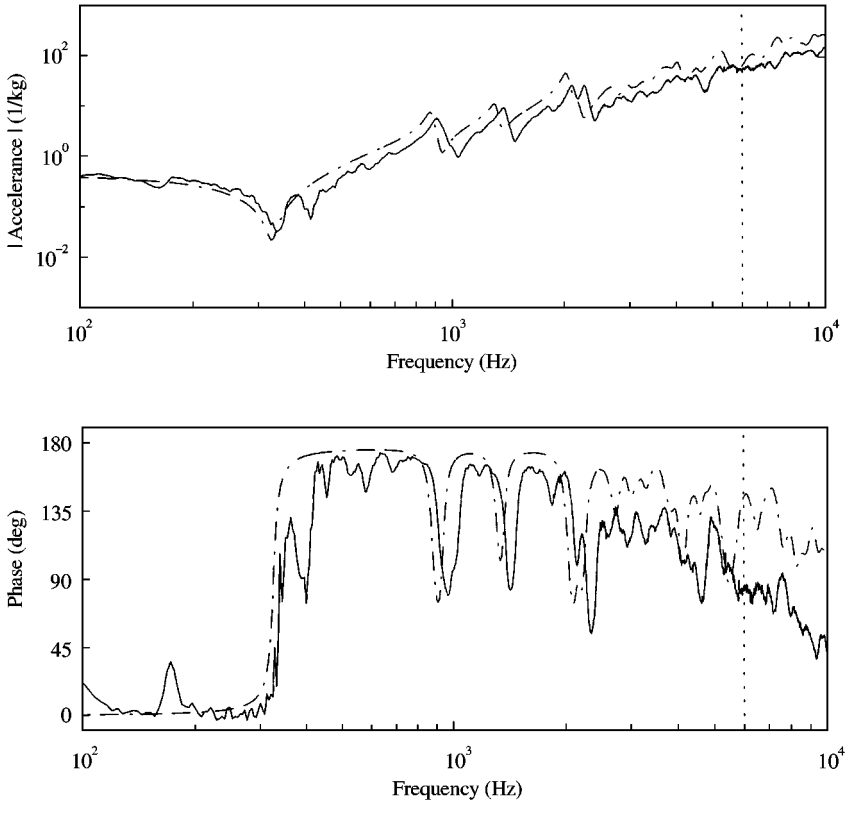

Figure 8. Input accelerance at node 1 in the z direction for the perspex box: ——, exciter measurement; - - - -, membrane mesh prediction; ....., membrane mesh shear limit.

(iv) Above 2 kHz the measured phase begins to deviate from that predicted. Above 6 kHz (shown by the vertical dotted line) the measured phase suggests the existence of a travelling wave. This is most probably due to the small distance between the exciter and the accelerometer. The difference may also be exacerbated by the deficiency of the membrane shear motion above 6 kHz.

The agreement between the prediction and the measurement in the rigid-body range means that the difference in the frequency average values above 400 Hz cannot be caused by a calibration error. In an effort to identify the cause of this discrepancy an additional drive-point measurement was made using an impact hammer to provide the excitation force. Figure 9 compares this hammer measurement with the predicted input accelerance from Figure 8. The hammer measurement is restricted to 4 kHz due to limited input force but predicts the frequency average value more accurately than the measurement with the electrodynamic exciter. This result suggests that the electrodynamic exciter includes a bias error.

The hammer measurement also predicts the prominent in-plane resonances more accurately than the exciter measurement. To investigate this difference, a second impact hammer measurement was made under nominally identical conditions about 2 years after that shown in Figure 9. Figure 10 compares the first and second hammer measurements. While the rigid-body and frequency average characteristics are identical, there are clear

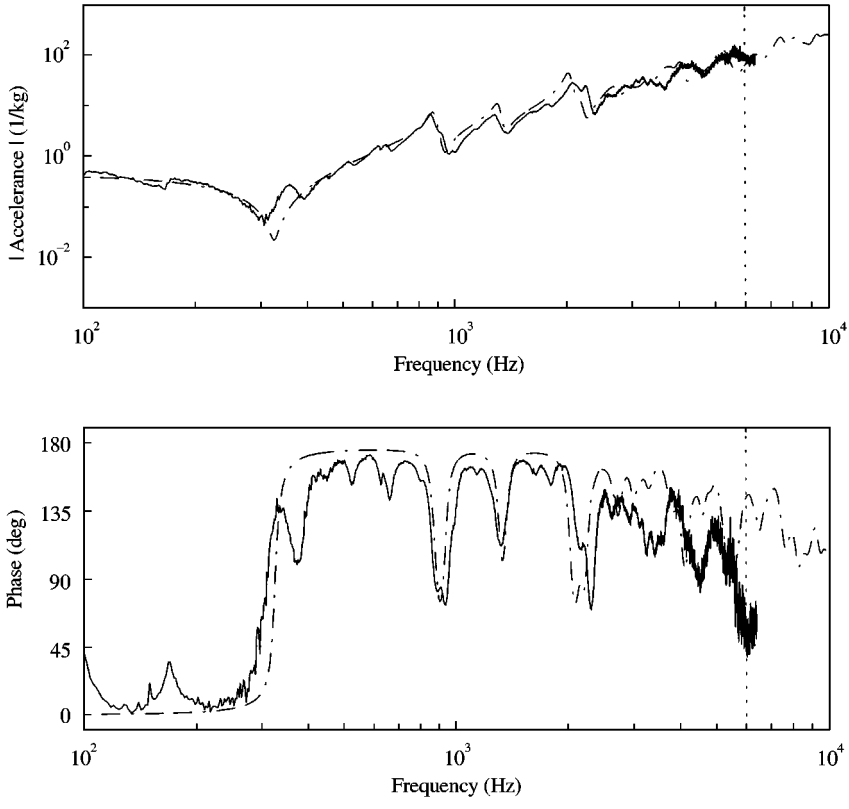

Figure 9. Input accelerance for the perspex box: ——, impact hammer measurement; - - - -, membrane mesh prediction; ....., membrane mesh shear limit.

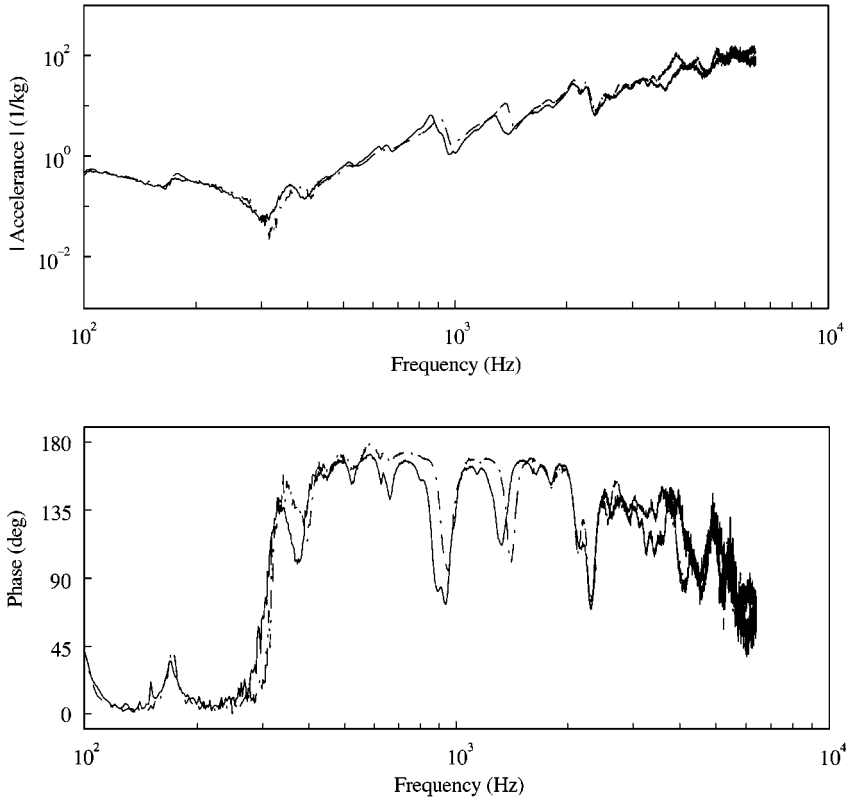

Figure 10. Comparison of the two input accelerance measurements made using the impact hammer; ——, 1st measurement; - - - -, 2nd measurement.

differences in the values and amplitudes of the prominent resonances. This comparison indicates that the mechanical properties of the perspex box are time-variant which accords with observations in reference [13] on structures made from materials similar to perspex. In this context, the 5% difference between the predicted and measured in-plane resonances observed in Figure 8 is not significant.

Figure 11 compares the characteristic membrane accelerance derived from equation (6), the imaginary part of the membrane mesh prediction and the measurement made using the electrodynamic exciter. The following observations are made.

(i) In the rigid-body region below 320 Hz, the imaginary part of the measurement has some negative values due to inadequate signal from the accelerometer.

(ii) In Figure 11(a), the characteristic accelerance is a good frequency average of the measurement up to 8 kHz. Above this frequency, the measurement starts to fall which is expected to be due to the separation of the accelerometer and the exciter and the effects of damping.

(iii) In Figure 11(b), the predicted imaginary part compares quite favourably with the measurement up to 2·5 kHz with the exception of the flexural resonances which, as expected, are not predicted. Above 2·5 kHz, the two curves are in reasonable agreement until 7 kHz whereupon the prediction lies consistently above the

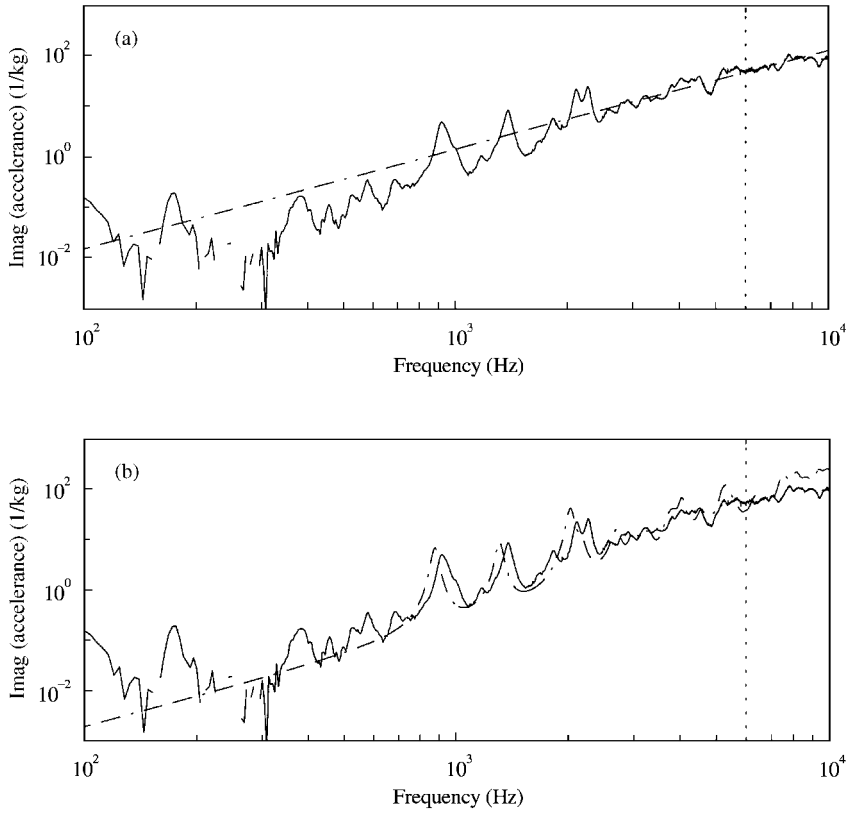

Figure 11. Imaginary parts of the perspex box input accelerance: ——, measurement; - · - · -, prediction; ....., membrane mesh shear limit. (a) Comparison with characteristic membrane accelerance (equation (6)); (b) comparison with membrane mesh accelerance.

measurement. This difference is expected to be due to the inaccurate modelling of the shear motion above 6 kHz.

The conclusion from these measurements is that the membrane mesh does estimate the dominant input accelerance of the perspex box quite accurately, especially in the range in which the shear motion is modelled sufficiently well. In the region where the shear motion is not well described the prediction appears to deteriorate, although the degradation in the performance of the membrane mesh is not particularly marked.

6.2. TRANSFER ACCELERANCES

There are almost as many transfer accelerance predictions as there are degrees of freedom on the membrane model. In this section, just three transfer accelerances are compared with measurements made using the electrodynamic exciter. Reference [18] contains additional measurements.

Figures 12–14 compare the three transfer accelerance predictions and measurements at nodes 2–4 in the directions shown by the arrows in Figure 6. The locations were chosen to cover a range of points which were both near to and far from the drive point and which had various directions relative to that of the excitation force. However, all the locations are

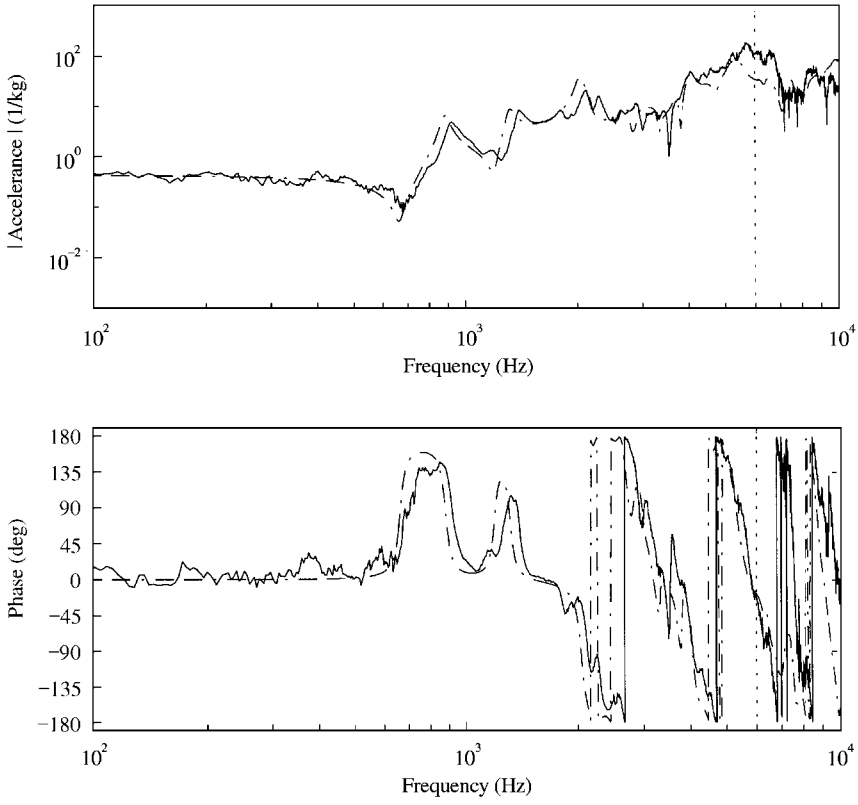

Figure 12. Transfer accelerance to node 2 in the z direction: ——, measurement; - · - · -, membrane mesh prediction; ....., membrane mesh shear limit.

situated at the edges of the box where the response is expected to be dominated by the in-plane motion. The following observations of Figures 12–14 are made:

(i) The predicted and measured magnitudes of all three graphs agree well in both the frequency average sense and at the peak and trough levels. The phase curves are also in acceptable agreement.
(ii) All the predictions and measurements share a number of prominent in-plane resonances. In addition, the measurements show poorly defined resonances attributable to flexural waves, but as in the case of the input measurement these additional resonances are difficult to resolve above 3 kHz.
(iii) The measurement in Figure 14 shows a resonance at 900 Hz which is not predicted. This probably represents a torsional mode which occurs in the measurement because the perspex box is not geometrically perfect.
(iv) All the graphs highlight the 6 kHz frequency above which the membrane mesh shear motion is expected to be less well described, but none indicate that the mesh degrades significantly above 6 kHz.

These results strongly support the membrane mesh. The agreement in the peak and trough levels in all the comparisons suggests that the inherent damping of the in-plane waves is the dominant dissipation mechanism across the whole frequency range shown. This indicates perhaps that the analysis of Section 3 has overestimated the frequency below which the

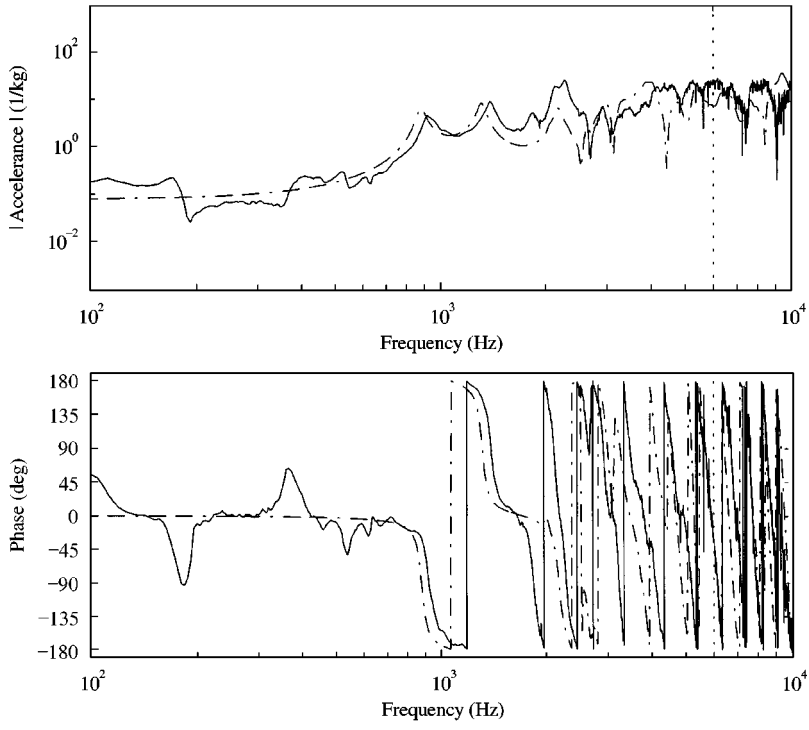

Figure 13. Transfer accelerance to node 3 in the x direction: ——, measurement; - · - · -, membrane mesh prediction; ....., membrane mesh shear limit.

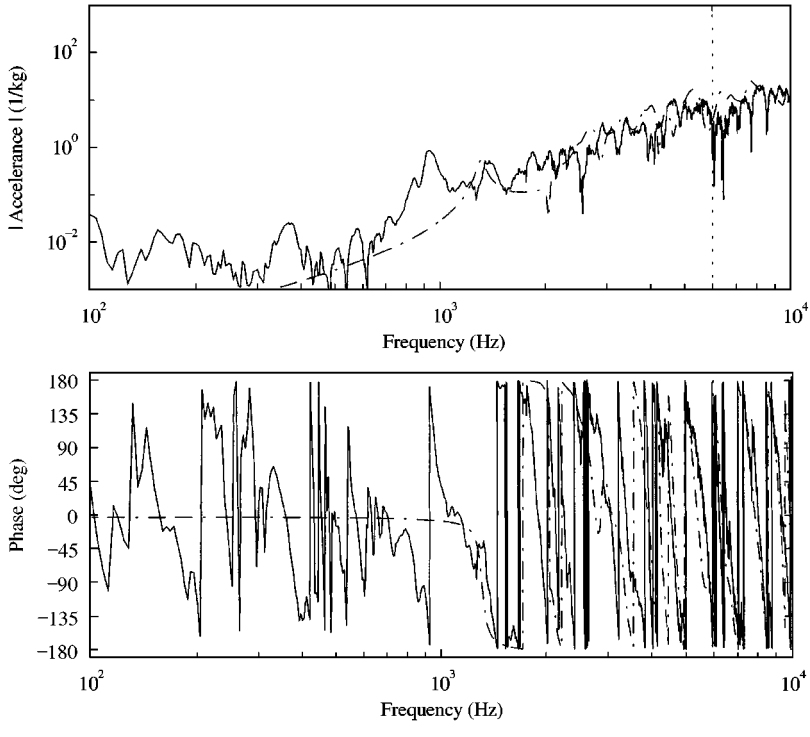

Figure 14. Transfer accelerance to node 4 in the y direction: ——, measurement; - · - · -, membrane mesh prediction; ....., membrane mesh shear limit.

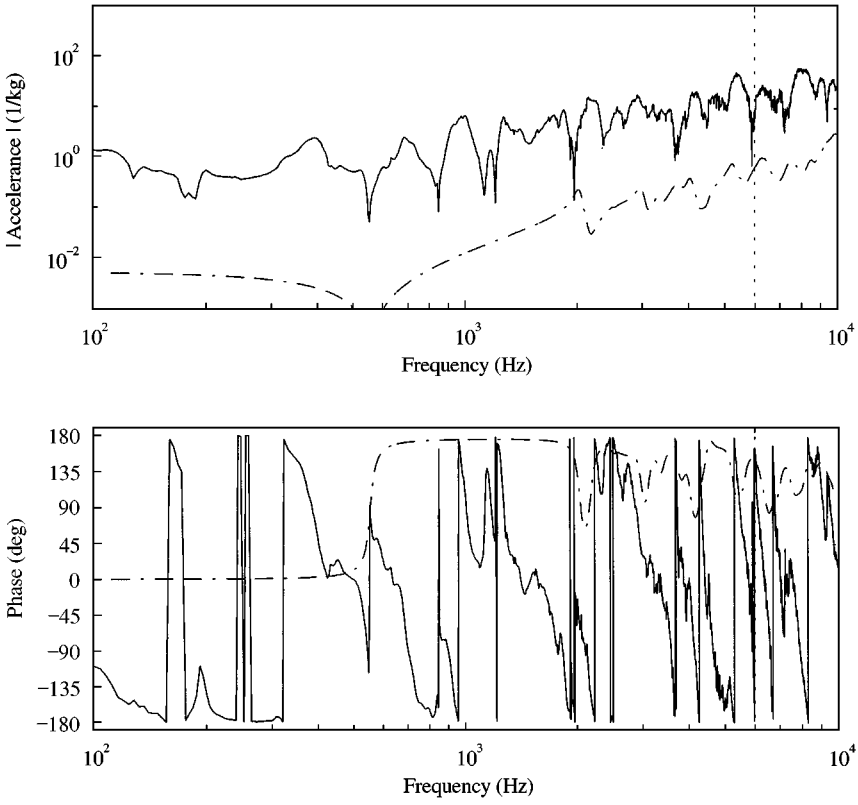

Figure 15. Transfer accelerance to node 5 in the z direction: ——, measurement; - · - · -, membrane mesh prediction; ....., membrane mesh shear limit.

damping of the structure is controlled by transmission of energy from in-plane to flexural waves at the joints.

Finally, and merely out of curiosity, it was decided to examine the behaviour of the membrane mesh in predicting the response at a point whose motion is *not* expected to be dominated by the in-plane motion. One such location is the response at node 5 in the z direction of Figure 6. Figure 15 compares the transfer accelerance predicted by the membrane mesh at this point with the corresponding measurement. It is clear that the prediction is woefully inaccurate but of course this is not unexpected because the membrane model was never intended to predict this type of response.

7. CONCLUSIONS

It has been shown that the built-up thin-plate box structure of Figure 1 when driven by a force at the edge where two plates meet possesses the following characteristics.

(i) The input response is dominated by the membrane mobility of equation (6) (or its corresponding impedance). This dominance is due to the much larger wavelength of the in-plane waves compared to the wavelength of the flexural waves and has been verified over the frequency ranges encountered in practical thin-plate structures.

(ii) Consideration of the dissipation mechanisms in the box and in practical thin-plate structures generally has shown that the damping produced by the transmission of in-plane energy to flexural energy at joints is likely to be important in controlling the in-plane response below a frequency defined by equation (18).

A finite element mesh of the edge-excited box has been constructed using membrane elements to model only the dominant in-plane motion. Below 6 kHz, four elements per wavelength were required to model the in-plane shear motion, but the same number of elements could model the in-plane quasi-longitudinal motion up to 10 kHz due to their longer wavelengths. In comparison with measurements made on a perspex box using an electrodynamic exciter to drive the box to 10 kHz, the predicted input and transfer responses at the edges of the membrane mesh compared very favourably. The measurements exhibited more resonances than predicted, the additional ones being attributable to flexural motion which was specifically excluded by the membrane mesh. There was not any appreciable decrease in the level of agreement in the range above 6 kHz in which the in-plane shear motion was not well described. The results suggest that a membrane mesh of a built-up structure which is excited in-plane at its drive points can be used to estimate the dominant in-plane response of similarly excited practical structures.

REFERENCES

1. *Automotive Handbook* 1992 Stuttgart: ROBERT BOSCH GmbH
2. B. A. T. PETERSSON 1983 *Journal of Sound and Vibration* **91**, 219–238. An approximation for the point mobility at the intersection of two perpendicular plates.
3. L. CREMER, M. HECKL and E. E. UNGAR 1988 *Structure-Borne Sound*. Berlin: Springer-Verlag, second edition.
4. B. M. GIBBS and P. G. CRAVEN 1981 *Journal of Sound and Vibration* **77**, 429–435. Sound transmission and mode coupling at junctions of thin plates. Part II: parametric survey.
5. E. E. UNGAR 1973 *Journal of Sound and Vibration* **26**, 141–154. The status of engineering knowledge concerning the damping of built-up structures.
6. S. K. JHA 1976 *Journal of Sound and Vibration* **47**, 543–558. Characteristics and sources of noise and vibration and their control in motor cars.
7. J. D. DIXON and A. V. PHILLIPS 1989 *Proceedings Autotech*, Birmingham, England. In-vehicle engine noise simulation.
8. P. E. GECK and D. TAO 1992 *Proceedings of the 2nd International Conference on Vehicle Comfort, October, Bologna, Italy*. Body structures noise and vibration design guidance.
9. N. LALOR and G. STIMPSON 1992 *Proceedings of the 2nd International Conference on Vehicle Comfort, October, Bologna, Italy*, FEM + SEA + optimisation = low noise.
10. R. J. PINNINGTON 1988 *Technical Report No.* 162, *ISVR, Southampton University*. Approximate mobilities of built-up structures.
11. R. S. LANGLEY and K. H. HERON 1990 *Journal of Sound and Vibration* **143**, 241–253. Elastic wave transmission through plate/beam junctions.
12. H. KUTTRUFF 1979 *Room Acoustics*. London: Applied Science, second edition.
13. E. SKUDRZYK 1968 *Simple and Complex Vibratory Systems*. PA: Pennysylvania State University Press.
14. *ANSYS Theory Manual* Houston, USA: Swanson Analysis System Inc.
15. M. PETYT 1990 *Introduction to Finite Element Vibration Analysis*. Cambridge: Cambridge University Press.
16. F. J. FAHY 1994 *Philosophical Transactions of the Royal Society of London A* **346**, 431–447. Statistical energy analysis: a critical overview.
17. *ICI CHEMICAL AND POLYMERS LTD*. Darwen, Lancashire, England.
18. R. M. GRICE 1998 *Ph.D. Thesis, Southampton University*. Vibration analysis of built-up structures by combining finite element analysis and analytical impedances.

APPENDIX A: LIST OF SYMBOLS

b	width (m)
c	phase velocity (m/s)
D	beam stiffness (N m^2); plate stiffness (N m)
E	Young's modulus of elasticity (N/m^2)
$\bar{E}$	total time-averaged energy of vibration (N m)
f	circular frequency (Hz)
j	$=\sqrt{-1}$
k	wavenumber (m^{-1})
L	length (m)
m'_b	mass per unit length (kg/m)
m''_p	mass per unit area (kg/m^2)
N	finite element shape function
p, q	finite element co-ordinates (dimensionless)
$\bar{P}$	time-averaged power (Nm/s)
t	time (s); thickness (m)
u, w	displacement (m)
v	velocity (m/s)
x, y, z	general co-ordinates (m)
Y	structural mobility (m/s/N)
Z'	structural impedance per unit length (N s/m^2)
Δ	distance between transducers (m)
ε	generalized finite element co-ordinate
ζ	viscous loss factor (dimensionless)
η	structural loss factor (dimensionless)
ν	Poisson's ratio (dimensionless)
ρ	density (kg/m^3)
ω	radian frequency (rad/s)